

Alma Mater Studiorum Università di Bologna
Archivio istituzionale della ricerca

Viscous heating of a laminar flow in the thermal entrance region of a rectangular channel with rounded corners and uniform wall temperature

This is the final peer-reviewed author's accepted manuscript (postprint) of the following publication:

Published Version:

Suzzi N., Lorenzini M. (2019). Viscous heating of a laminar flow in the thermal entrance region of a rectangular channel with rounded corners and uniform wall temperature. INTERNATIONAL JOURNAL OF THERMAL SCIENCES, 145, 1-10 [10.1016/j.ijthermalsci.2019.106032].

Availability:

This version is available at: <https://hdl.handle.net/11585/725621> since: 2024-05-30

Published:

DOI: <http://doi.org/10.1016/j.ijthermalsci.2019.106032>

Terms of use:

Some rights reserved. The terms and conditions for the reuse of this version of the manuscript are specified in the publishing policy. For all terms of use and more information see the publisher's website.

This item was downloaded from IRIS Università di Bologna (<https://cris.unibo.it/>).
When citing, please refer to the published version.

(Article begins on next page)

This is the final peer-reviewed accepted manuscript of:

Viscous heating of a laminar flow in the thermal entrance region of a rectangular channel with rounded corners and uniform wall temperature / Suzzi N.; Lorenzini M.. - In: INTERNATIONAL JOURNAL OF THERMAL SCIENCES. - ISSN 1290-0729. - ELETTRONICO. - 145:(2019), pp. 106032.1-106032.10. [10.1016/j.ijthermalsci.2019.106032]

The final published version is available online at:

<https://dx.doi.org/10.1016/j.ijthermalsci.2019.106032>

Terms of use:

Some rights reserved. The terms and conditions for the reuse of this version of the manuscript are specified in the publishing policy. For all terms of use and more information see the publisher's website.

This item was downloaded from IRIS Università di Bologna (<https://cris.unibo.it/>)

When citing, please refer to the published version.

Viscous Heating of a Laminar Flow in the Thermal Entrance Region of a Rectangular Channel with Rounded Corners and Uniform Wall Temperature

Nicola Suzzi^a, Marco Lorenzini^{b,*}

^a*University of Udine - Department of Electrical, Management and Mechanical Engineering Udine, Via delle Scienze 206, I-33100 Udine (UD), ITALY*

^b*Alma Mater Studiorum - University of Bologna. DIN - Department of Industrial Engineering, Forlì Campus, Via Fontanelle 40, I-47121 Forlì (FC), ITALY*

Abstract

The numerical solution of Graetz-Brinkman problem is obtained for channels having rectangular cross section with rounded corners, under T boundary condition applied on the heated duct wall and adiabatic condition elsewhere, assuming an adiabatic preparation of the fluid at the inlet section. Several simulations are conducted and both Poiseuille and Nusselt numbers calculated, based on the computed velocity and temperature profiles. The numerical method is first verified with the resulting Nusselt and Poiseuille numbers with literature data, available for simplified configurations and fully developed flow, showing an excellent agreement. Comparison with numerical data is also conducted in case of fully developed flow and non-negligible viscous dissipation. A further validation is carried out comparing current computations with both experimental and numerical data in case of ther-

*Corresponding Author

Email addresses: `suzzi.nicola@spes.uniud.it` (Nicola Suzzi),
`marco.lorenzini@unibo.it` (Marco Lorenzini)

mally developing flow inside a rectangular channel with negligible viscous heating (i.e. the well-known Graetz problem).

The effects of duct cross section geometry and Brinkman number are investigated and new correlations, useful for the design of microchannel heat sinks, are presented in order to predict the Poiseuille number and average Nusselt numbers.

Keywords: Microchannel, Graetz Problem, Viscous heating, Microconvection

1. Introduction

Microchannels are employed in a broad range of engineering applications. For example, heat sinks belonging to the so-called MFDs (micro-flow devices) are largely used for integrated cooling of small electronic components. New manufacturing processes, often originated in the semiconductor industry, allow fabrication of non-conventional silicon structures and channels of several cross-sections, [1], which, in turn, has given a new impulse to the investigation of single phase laminar forced convection through channels of various shapes, as testified by the literature. In fact, several research works investigate basic phenomena driving heat transfer and fluid flow in microchannels [2–14] and propose effective 1st- and 2nd-law based methods for optimization of channel geometry [15–20]. In [6] heat transfer through square and rectangular channels with rounded corners was numerically investigated: assuming fully developed flow, negligible axial conduction and applying H1 boundary conditions, the authors solved the governing Navier-Stokes equations over the 2D channel cross section domain and proposed new correlations for Poiseuille

17 and Nusselt numbers as a function of joint radius. Temperature field in the
18 restrictive case of rectangular channel section geometry and H2 boundary
19 condition was analitically calculated in [2] and the resulting Nusselt number
20 computed for different aspect ratios. A semi-analytical approach was used
21 by Ray et al. [21] in order to solve the governing equations for a fully de-
22 veloped flow through square and equilateral triangular ducts with rounded
23 corners under H1 and H2 boundary conditions. The influence of rarefaction
24 on the Poiseuille number was numerically [7, 22], analytically [9] and exper-
25 imentally [10] studied for rectangular, trapezoidal and elliptical ducts, with
26 velocity-slip conditions being applied at the duct wall.

27 The effect of viscous dissipation in laminar forced convection through mi-
28 crochannels was studied by Morini [3] and a criterion to draw the limit of
29 significance for viscous heating presented, while modified correlations for
30 Nusselt number as a function of Brinkman number were presented in [5]:
31 the author considered a fully developed flow through rectangular rounded
32 channels with H1 boundary conditions and assumed non-negligible viscous
33 heating effect. The combined effect of viscous dissipation and rarefied flow
34 was studied in [8], where 2D Navier-Stokes equations for a fully developed
35 flow through an elliptical channel are numerically solved by means of **COMSOL**
36 **Multiphysics**[®], applying velocity-slip condttion due to rarefaction effect
37 and H2 thermal boundary condition; Nusselt number is thus traced as a
38 function of both Knudsen and Brinkman numbers. A similar problem, i.e.
39 fully developed flow through rectangular-shaped channels and non-negligible
40 viscous heating, was numerically investigated by Barletta et al. [23], who
41 solved the governing equations with H1 and T thermal boundary conditions

42 using FlexPDE[®] and studied the effect of channel aspect ratio on the com-
43 puted Nusselt number.

44 In the area of single phase laminar forced convection a number of scientific
45 papers deals with thermally developing flow through channels, i.e. the so-
46 called Graetz problem, which was solved analytically by Graetz and Nusselt
47 more than a century ago in the simple case of circular ducts. An early work
48 about thermally developing, laminar flow was presented by Michelsen et al.
49 [24], who numerically investigated the extended Graetz problem for a fluid
50 flowing in a circular tube with imposed wall temperature and uniform inlet
51 temperature profile, when axial heat conduction cannot be neglected. The
52 numerical results were presented in terms of local Nusselt number as a func-
53 tion of axial coordinate for different values of the non-dimensional Peclet
54 number. A different extension of the Graetz problem was investigated in
55 [25]: the authors assumed negligible axial heat conduction, but included the
56 effect of viscous dissipation in the energy equation leading to the so-called
57 Graetz-Brinkman problem, which may occur when micro-scales are involved.
58 Thus, the momentum and energy equations were analytically solved for a
59 circular tube, with both H2 and T boundary conditions being imposed at
60 the channel wall. The Nusselt number was then expressed as a function of
61 axial coordinate for different values of the Brinkman number, which com-
62 pares viscous heating and heat conduction. The Graetz-Brinkman problem
63 was also solved by Barletta et al. [23] in the case of parallel plates under
64 T boundary conditions and adiabatic preparation of the fluid flow. Adopt-
65 ing a semi-analytical approach, the temperature field was decomposed into
66 two contributions and the governing energy equation solved via separation

of variables, which leads to an eigenvalue problem. Laminar forced convection inside non-circular tubes was numerically studied in [26–28], where the canonical Graetz problem (i.e. negligible axial conduction and viscous heating) was solved for different boundary conditions: Aparecido and Cotta [26] proposed a semi-analytic solution in case of rectangular ducts with T boundary condition imposed at the duct wall and uniform inlet temperature; Lee and Garimella [27] used **ANSYS Fluent**[®] in order to simulate channels having rectangular cross section under H1 boundary conditions applied at channel wall; Filali et al. [28] considered a non-linear viscoelastic fluid and numerically investigated circular, equilateral triangular and rectangular cross sections under H2 and T boundary conditions, looking for the influence of rheological parameters on heat transfer.

Different extensions of the Graetz problem can be found in literature: Aydin and Avci [29] and Barışık et al. [30] solved the so-called micro-Graetz-Brinkman problem, i.e. non-negligible axial conduction, viscous dissipation and rarefaction effects, in the restrictive case of a circular duct, imposing generalized Neumann condition at the duct wall. Such a boundary condition derives from the slip on both temperature and velocity fields occurring at duct wall due to rarefaction.

The aim of this work is the solution of the Graetz-Brinkman problem. Assuming laminar forced convection of a Newtonian fluid, neglecting axial conduction and rarefaction but accounting for viscous heating, the governing Navier-Stokes and energy equations are solved numerically. Rectangular ducts with rounded corners and three or four heated edges are considered, with a T thermal boundary condition applied along the heated perimeter.

92 Following [23], the method of separation of variables is applied in order to
 93 reduce the three-dimensional physical problem to a two-dimensional mathe-
 94 matical problem, resulting in a more efficient numerical solution in terms of
 95 computational costs. The local Nusselt number is computed as a function
 96 of axial coordinate and the effect of relevant non-dimensional parameters
 97 analysed, providing new correlations for Nusselt number prediction. It is
 98 important to point out that such a test case has never been investigated
 99 before. In fact, heat transfer performance of rectangular rounded ducts was
 100 studied for laminar, fully developed flow in [6], under the assumption of negli-
 101 gible viscous heating effect and H1 thermal boundary condition along heated
 102 perimeter, while the thermally developing flow problem with non-negligible
 103 viscous heating has been solved for simplified geometries only [23, 29, 30].

104 2. Mathematical model

Assuming that an incompressible, Newtonian fluid flows through the channel in steady, laminar, hydrodynamically developed regime, subject to no-slip at the wall and T thermal boundary condition (fixed temperature T_w at the heated portion of the channel wall) and neglecting axial conduction (x denoting the axial, or streamwise, coordinate), momentum and energy equations give,

$$\mu \left(\frac{\partial^2 u}{\partial y^2} + \frac{\partial^2 u}{\partial z^2} \right) - \frac{\partial p}{\partial x} = 0 \quad (1)$$

$$\rho c_p u \frac{\partial T}{\partial x} = k \left(\frac{\partial^2 T}{\partial y^2} + \frac{\partial^2 T}{\partial z^2} \right) + \mu \Phi \quad (2)$$

105 Φ being the viscous dissipation function:

$$\Phi = \left(\frac{\partial u}{\partial y} \right)^2 + \left(\frac{\partial u}{\partial z} \right)^2 \quad (3)$$

106 It is convenient to express the pressure gradient $\frac{\partial p}{\partial x}$, which is constant along
 107 the whole channel length L under the assumption of hydrodynamically de-
 108 veloped flow, as a function of the friction factor and the bulk velocity:

$$\frac{\partial p}{\partial x} = \frac{\Delta p}{L} = \frac{1}{2} f \rho u_b^2 \frac{1}{D_h} \quad (4)$$

The following boundary conditions are applied at the channel wall:

$$u|_P = 0 : \text{no-slip condition at wall;} \quad (5)$$

$$T|_{P_h} = T_w : \text{fixed temperature along heated perimeter;} \quad (6)$$

$$\nabla T \cdot \hat{\mathbf{n}} = 0 : \text{adiabatic condition through } P - P_h. \quad (7)$$

109 The inlet temperature profile $T|_{x=0} = T_0(x, y)$ must be also imposed. Differ-
 110 ent inlet conditions may be investigated:

- 111 • uniform temperature profile, namely T_i , is usually imposed in the avail-
 112 able literature dealing with Graetz problem;
- 113 • an adiabatic preparation of the fluid was introduced by Barletta et al.
 114 [23] for solving the Graetz-Brinkman problem in case of parallel plates,
 115 since it should lead to a more realistic configuration than a flat profile.

116 The same approach as [23] is here adopted. Thus, assuming an adiabatic
 117 preparation of the fluid, the energy equation at leading viscous effect,

$$k \left(\frac{\partial^2 T_0}{\partial y^2} + \frac{\partial^2 T_0}{\partial z^2} \right) + \mu \Phi = 0 \quad (8)$$

118 must be solved under adiabatic condition imposed along the channel section
 119 perimeter,

$$\nabla T_0 \cdot \hat{\mathbf{n}} = 0 \text{ through } P \quad (9)$$

in order to provide the inlet temperature profile $T_0(y, z)$.

By defining the following non-dimensional quantities,

$$\xi = \frac{x}{L}; \eta = \frac{y}{D_h}; \zeta = \frac{z}{D_h} \quad (10)$$

$$\tilde{u} = \frac{u}{u_b}; \tilde{\Phi} = \left(\frac{D_h}{u_b}\right)^2 \Phi; \tilde{p} = \frac{\partial p}{\partial x} \frac{D_h^2}{\mu u_b}; \Theta = \frac{T - T_w}{T_w - T_i} \quad (11)$$

and introducing the Brinkman, Graetz and Poiseuille numbers,

$$\text{Br} = \frac{\mu u_b^2}{k (T_w - T_i)}; \text{Gz} = \text{Re Pr} \frac{D_h}{L}; \text{Po} = f \text{Re} \quad (12)$$

Equations (1) and (2) can be rewritten in a non-dimensional form:

$$\frac{\partial^2 \tilde{u}}{\partial \eta^2} + \frac{\partial^2 \tilde{u}}{\partial \zeta^2} = -2 \text{Po} \quad (13)$$

$$\text{Gz} \tilde{u} \frac{\partial \Theta}{\partial \xi} = \left(\frac{\partial^2 \Theta}{\partial \eta^2} + \frac{\partial^2 \Theta}{\partial \zeta^2} \right) + \text{Br} \tilde{\Phi} \quad (14)$$

Boundary conditions can also be expressed in a non-dimensional fashion:

$$\tilde{u}|_{\partial\Omega} = 0 : \text{no-slip condition at wall}; \quad (15)$$

$$\Theta|_{\partial\Omega_h} = 0 : \text{fixed temperature along heated perimeter}; \quad (16)$$

$$\nabla \Theta \cdot \hat{\mathbf{n}} = 0 : \text{adiabatic condition elsewhere, } \partial\Omega - \partial\Omega_h. \quad (17)$$

120 3. Temperature problem and Nusselt number

121 Following the approach of [23], the solution of Eqs. (13) and (14), subject
122 to no-slip condition at wall and fixed wall temperature, is sought in the form,

$$\Theta = \Theta_v + \Theta_c \quad (18)$$

123 where:

- Θ_v is the ξ -independent solution of the partial differential equation describing the effects of viscous heating on the temperature field

$$\frac{\partial^2 \Theta_v}{\partial \eta^2} + \frac{\partial^2 \Theta_v}{\partial \zeta^2} + \text{Br} \tilde{\Phi} = 0 \quad (19)$$

$$\tilde{\Phi} = \left(\frac{\partial \tilde{u}}{\partial \eta} \right)^2 + \left(\frac{\partial \tilde{u}}{\partial \zeta} \right)^2 \quad (20)$$

124 with uniform wall temperature imposed along the heated perimeter and
125 adiabatic conditions everywhere else;

- Θ_c is the solution of the energy equation with negligible viscous heating effect,

$$\text{Gz} \tilde{u} \frac{\partial \Theta_c}{\partial \xi} = \frac{\partial^2 \Theta_c}{\partial \eta^2} + \frac{\partial^2 \Theta_c}{\partial \zeta^2} \quad (21)$$

with uniform wall temperature imposed along the heated perimeter and adiabatic conditions elsewhere too over the channel wall. According to adiabatic preparation of the fluid, the additional inlet temperature profile, $\Theta|_{\xi=0} = \Theta_0(\eta, \zeta)$ is obtained via the solution of:

$$\frac{\partial^2 \Theta_0}{\partial \eta^2} + \frac{\partial^2 \Theta_0}{\partial \zeta^2} + \tilde{\Phi} = 0 \quad (22)$$

$$\nabla \Theta_0 \cdot \hat{\mathbf{n}} = 0 \text{ on } \partial \Omega \quad (23)$$

128 Following [23], Θ_c can be computed via separation of variables,

$$\Theta_c = \sum_{n=0}^{+\infty} C_n \alpha_n(\xi) \psi_n(\eta, \zeta) \quad (24)$$

129 where C_n are constants depending on the prescribed temperature distribution
130 imposed at the inlet section and α_n is equal to:

$$\alpha_n = \exp \left(-\frac{\lambda_n}{\text{Gz}} \xi \right) \quad (25)$$

131 Thus, Eq. (21) can be reduced to the following eigenvalue problem,

$$\frac{\partial^2 \psi_n}{\partial \eta^2} + \frac{\partial^2 \psi_n}{\partial \zeta^2} + \lambda_n \tilde{u} \psi_n = 0 \quad (26)$$

132 with a T thermal boundary condition imposed along the heated perimeter:

$$\begin{aligned} n &= 0 \text{ on } \partial\Omega_h \\ \nabla \psi_n \cdot \hat{\mathbf{n}} &= 0 \text{ on } \partial\Omega - \partial\Omega_h \end{aligned} \quad (27)$$

133 Equations (13), (19) and (26) must be solved and the coefficients C_n and
134 eigenvalues λ_n computed, yielding the velocity field $\tilde{u}(\eta, \zeta)$ and the temper-
135 ature field $\Theta(\xi, \eta, \zeta)$.

136 Thus, the average Nusselt number can be computed over the channel length
137 as,

$$\text{Nu} = \frac{q_w D_h}{k (T_w - T_b)} \quad (28)$$

138 where q_w represents the average heat flux through wall, defined through
139 integration of the Fourier law along channel section perimeter,

$$q_w = -\frac{k (T_w - T_i)}{D_h} \frac{1}{\partial\Omega_h} \int_{\partial\Omega} \nabla \Theta \cdot \hat{\mathbf{n}} d\Gamma \quad (29)$$

140 with $d\Gamma = \frac{dl}{D_h}$ the non-dimensional tangential direction to the cross-section
141 perimeter.

142 Following [23], the non-dimensional temperature can be decomposed accord-
143 ing to Eq. (18) and the average Nusselt number reduced to,

$$\text{Nu} = \frac{\text{Nu}_v \Theta_{b,v} + \text{Nu}_c \Theta_{b,c}}{\Theta_{b,v} + \Theta_{b,c}} \quad (30)$$

144 where:

- Nu_v , which is the Nusselt number related to viscous heating, can be calculated as,

$$\text{Nu}_v = \frac{\frac{1}{\partial\Omega_h} \int_{\Omega} \text{Br} \tilde{\Phi} d\Omega}{\Theta_{b,v}} \quad (31)$$

$\Omega = A_c/D_h^2$ being the non-dimensional channel section area, $\partial\Omega_h$ the non-dimensional heated perimeter and $\Theta_{b,v}$ the bulk temperature:

$$\Theta_{b,v} = \frac{\int_{\Omega} \tilde{u} \Theta_v d\Omega}{\int_{\Omega} \tilde{u} d\Omega} \quad (32)$$

- Nu_c , which is the Nusselt number resulting from solution of the eigenvalue problem described by Eq. (26), is given by:

$$\text{Nu}_c = \frac{\sum_{n=0}^{+\infty} \left(\frac{\lambda_n P_h}{4 P} \right) b_{n} \exp \left(-\frac{\lambda_n}{\text{Gz}} \xi \right)}{\Theta_{b,c}} \quad (33)$$

λ_n corresponds to the n -th eigenvalue, with ψ_n the n -th eigenfunction.

Thus, we have:

$$b_{n} = \frac{C_n \int_{\Omega} \tilde{u} \psi_n d\Omega}{\int_{\Omega} \tilde{u} d\Omega} \quad (34)$$

$\Theta_{b,c}$ is the bulk temperature, which depends on channel axial coordinate

ξ according to:

$$\Theta_{b,c} = \sum_{n=0}^{+\infty} b_{n} \exp \left(-\frac{\lambda_n}{\text{Gz}} \xi \right) \quad (35)$$

Computing Nu_v through Eq. (31), i.e. using the total thermal power generated by viscous dissipation, which is an integral quantity, and the bulk temperature, rather than integrating the local heat flux through the heated perimeter, ensures a more accurate estimation when post-processing numerical data. For the same reason, it is convinient to compute Nu_c through Eq. (33), which refers to integral quantities too. It is also worth pointing out that the mean Nusselt number at negligible viscous heating for a fully developed

162 flow (i.e. at a distance $x \rightarrow \infty$ from the inlet section) can be calculated,
 163 according to Eq. (33), as a function of the first eigenvalue λ_1 :

$$\text{Nu}_c \xrightarrow{x \rightarrow \infty} \frac{\lambda_1}{4} \frac{P_h}{P} \quad (36)$$

164 4. Numerical method

165 Governing equations, Eqs. (13), (19) and (26) can not be analitically
 166 solved but in few cases: circular and rectangular channel cross-sections, with
 167 Green's functions generally used in the latter case. Since we want to inves-
 168 tigate the effect of smoothing the corners of a partially heated rectangular
 169 shaped channel (leading to a more complex geometry, as shown in figure 1), a
 170 numerical approach must be adopted in order to assess both the velocity and
 171 temperature fields. Thus, Eqs. (13), (19) and (26) are numerically solved
 172 using the available FEM solvers and mesh generator included in the pdetool
 173 package of **MATLAB**[®]. An initial triangular mesh discretizing the 2D channel
 174 section is first generated.

175 Solution of momentum equation, Eq. (13), is iterated until the guessed
 176 Poiseuille number is such that

$$\text{Po} : \tilde{u}_b = \frac{1}{\Omega} \int_{\Omega} \tilde{u} d\Omega \simeq \frac{1}{\Omega} \sum_{i=1}^{n_e} \tilde{u}_i d\Omega_i = 1 \quad (37)$$

177 with $i \in [1, n_e]$ denoting the i -th mesh element. The energy equation for vis-
 178 cous heating, Eq. (19), with imposed wall temperature is numerically solved
 179 on the same mesh grid as that for Eq. (13) since the velocity field is required
 180 to compute viscous dissipation function. The **MATLAB**[®] function `@adaptmesh`
 181 is used in order to solve Eqs. (13) and (19) with an adaptive triangular mesh
 182 method, the initial mesh being progressively refined in order to get a more

183 accurate solution.

184 The eigenvalue problem, given by Eqs. (26) and (27), is solved using `@pdeeig`,
185 which returns both the eigenvalues λ_n and the eigenfunctions ψ_n , on the same
186 mesh as that employed for momentum equation, Eq. (13), with the velocity
187 field being required to compute the non-linear coefficient in Eq. (26).

188 Once the eigenfunctions ψ_n , the corresponding eigenvalues λ_n and the tem-
189 perature field for viscous heating Θ_v are computed, the coefficients C_n can
190 be determined so as to satisfy the imposed inlet temperature distribution
191 (the function `@lsqnonlin`, belonging to the **MATLAB**[®] optimization toolbox,
192 is used for such a purpose), allowing to calculate the non-dimensional tem-
193 perature field Θ inside the channel as:

$$\Theta = \Theta_v(\eta, \zeta) + \sum_n C_n \psi_n(\eta, \zeta) \exp\left(-\frac{\lambda_n}{Gz} \xi\right) \quad (38)$$

194 Since decomposing temperature field into two contributions, Eq. (18), and
195 applying separation of variables, Eq. (24), leads to two PDEs to be solved
196 on a 2D computational domain together with momentum PDE, the pro-
197 posed numerical procedure is much more efficient than a fully 3D approach
198 in terms of computational costs, allowing for investigation of a wide range of
199 configurations.

200 5. Investigated setup

201 Two different sets of geometry describing real configurations are investi-
202 gated:

- 203 • 3T: channel section identified by a rectangular shape with 2 rounded
204 corners, Fig. 1(a);

- 4T: channel section identified by a rectangular shape with 4 rounded corners, Fig. 1(b).

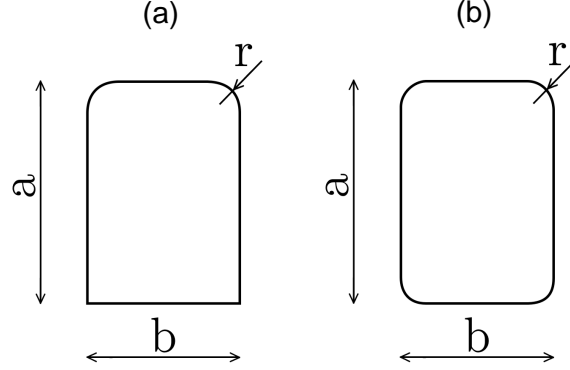


Figure 1: Investigated channel geometries: rectangular shape with 2 rounded corners (a); rectangular shape with 4 rounded corners (b).

Geometry characteristics are identified in terms of aspect ratio β and non-dimensional radius of curvature γ ,

$$\beta = \frac{b}{a}; \gamma = 2 \frac{r}{b} \quad (39)$$

with b the shorter edge of the reference rectangular cross-section.

The no-slip condition at channel wall is used in all instances,

$$\tilde{u}|_{\partial\Omega} = 0 \quad (40)$$

whilst two different sets of boundary conditions concerning temperature field are investigated:

- referring to Fig. 1(a), the T boundary condition is imposed along the heated cross section perimeter, whilst the adiabatic condition is applied

215 on the short edge of the channel cross section having sharp corners,

$$\begin{aligned}\Theta|_{\partial\Omega_h} &= 0 \\ \nabla\Theta \cdot \hat{\mathbf{n}} &= 0 \text{ on } \partial\Omega - \partial\Omega_h\end{aligned}\tag{41}$$

216 $\hat{\mathbf{n}}$ being the normal inward direction to the duct cross section.

217 • referring to Fig. 1(b), wall temperature T_w is imposed along whole
218 channel cross section perimeter, leading to T boundary condition:

$$\Theta|_{\partial\Omega} = 0\tag{42}$$

219 Adiabatic preparation of the fluid is imposed and the inlet temperature pro-
220 file computed through Eqs. (22) and (23), with the non-dimensional viscous
221 dissipation function $\tilde{\Phi}$ in Eq. (22) estimated from the known developed ve-
222 locity profile. Since Eqs. (22) and (23) admit infinite solutions, the following
223 condition was imposed in order to compute inlet profile Θ_0 ,

$$\frac{1}{\Omega} \int_{\Omega} \tilde{u} \Theta_0 d\Omega = -1\tag{43}$$

224 which means that bulk temperature of incoming fluid corresponds to the
225 reference inlet temperature T_i .

226 6. Model verification and validation

227 6.1. Fully developed flow

228 The numerical procedure was first verified with some experimental results
229 from the literature, which cover simple geometry configurations. Comparison
230 with numerical results is also conducted when viscous heating and complex
231 coss-sectional geometry are involved. The Poiseuille and Nusselt numbers for

232 a fully developed flow through a rectangular cross-section with sharp corners,
 233 i.e. $\gamma = 0$, are available for different aspect ratios β , when viscous heating
 234 is negligible (i.e. $Br = 0$) and wall temperature imposed along 3 or 4 edges
 235 [31, 32]. Barletta et al. [33] numerically investigated the case of hydrody-
 236 namically and thermally developed flow through a channel with dominant
 237 viscous heating. The channel geometry was rectangular with four rounded
 238 corners, $\beta \in [0.05, 1]$ and $\gamma = 1$, and uniform wall temperature along the
 239 whole perimeter: under the above mentioned assumption, Nusselt number
 240 does not change along the axial coordinate and depends on the geometry
 241 of the channel's cross-section only, regardless of the the magnitude of the
 242 Brinkman number.

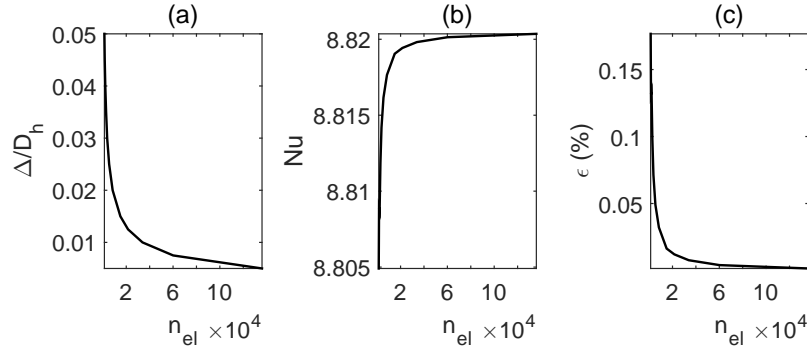


Figure 2: Mesh accuracy parameter versus number of triangular elements (a), developed Nusselt number (b) and estimation error (c) as a function of elements number. Test case 3T, $\beta = 3/5$, $\gamma = 2/3$.

243 After setting the accuracy of MATLAB[®] mesh generator in order to ensure
 244 grid independence (namely reached when computed Poiseuille and Nusselt
 245 numbers are no more affected by mesh progressive refinement), numerical
 246 results are compared to the results reported in [33] and [31] in terms of

247 both Poiseuille and Nusselt numbers. A grid dependence analysis was con-
 248 ducted: the accuracy parameter of MATLAB[®] gridder `@generateMesh` (i.e.
 249 the maximum distance between two neighbour nodes, namely Δ/D_h) was
 250 progressively increased and both average Nusselt number at leading viscous
 251 heating and estimation error were traced as a function of mesh elements, as
 252 shown in Fig. 2, finding a discrepancy of about 0.0076% on the estimated Nu
 253 when $\Delta/D_h = 10^{-2}$. Using adaptive mesh option, i.e. `@adaptmesh` function,
 254 always ensures higher accuracy than `@generateMesh` for a given number of
 255 mesh elements.

β	Po		Nu _v	
0.05	22.87 ^[33]	22.87	16.21 ^[33]	16.21
0.1	21.85 ^[33]	21.86	15.07 ^[33]	15.06
0.2	20.13 ^[33]	20.13	13.18 ^[33]	13.18
0.3	18.78 ^[33]	18.78	11.80 ^[33]	11.80
0.4	17.76 ^[33]	17.76	10.86 ^[33]	10.86
0.5	17.03 ^[33]	17.03	10.26 ^[33]	10.26
0.6	16.54 ^[33]	16.54	9.906 ^[33]	9.906
0.7	16.24 ^[33]	16.24	9.714 ^[33]	9.714
0.8	16.08 ^[33]	16.08	9.628 ^[33]	9.627
0.9	16.01 ^[33]	16.01	9.602 ^[33]	9.601
1	16.00 ^[33]	16.00	9.600 ^[33]	9.600

Table 1: Computed vs literature Poiseuille and Nusselt numbers in case of: dominant
 viscous heating; wall temperature imposed; 4T, $\gamma = 1$.

256 Tables 1 and 2 show a perfect agreement with both the numerical results



β	Po		Nu _c			
						
0.1	21.17 ^[31]	21.17	—	5.908	6.095 ^[31]	6.189
0.2	19.07 ^[31]	19.07	—	4.829	5.195 ^[31]	5.256
0.3	17.51 ^[31]	17.51	—	4.130	4.579 ^[31]	4.626
1/3	17.09 ^[31]	17.09	3.956 ^[31]	3.958	—	4.464
0.4	16.37 ^[31]	16.37	—	3.681	4.154 ^[31]	4.191
0.5	15.55 ^[31]	15.55	3.391 ^[31]	3.392	3.842 ^[31]	3.874
0.7	14.61 ^[31]	14.61	—	3.091	3.408 ^[31]	3.432
1/1.4	14.56 ^[31]	14.57	3.077 ^[31]	3.078	—	3.407
1	14.23 ^[31]	14.23	2.976 ^[31]	2.978	3.018 ^[31]	3.025

Table 2: Computed vs literature Poiseuille and Nusselt numbers in case of: negligible viscous heating; 3 and 4 heated edges; $\gamma = 0$.

257 of [33] and the analytical values of [31] in terms of Poiseuille number for all
 258 the geometries investigated. Computations of the Nusselt number at domi-
 259 nant viscous heating, Nu_v , also reveals sufficient accuracy compared to the
 260 numerical results of [33], as shown in Table 1, as well as the Nusselt num-
 261 ber at negligible viscous heating, Nu_c , whose estimation is verified with the
 262 literature, analytical values of [31] in case of rectangular cross section and 4
 263 heated edges, as shown in Table 2; Nu_c for a circular shape was also veri-
 264 fied to converge asymptotically to the well-known value of 3.66 for increasing
 265 mesh refinement. More uncertainty on the computed Nusselt number Nu_c
 266 was found when 3 edges are heated (with temperature imposed along the

267 heated perimeter and adiabatic condition imposed elsewhere), the discrep-
 268 ancy with values of [31] ranging between 0.2–1.5 % as clearly shown in Table
 269 2. However, such a discrepancy can be found even comparing literature re-
 270 sults of [31] with those of [32], when T boundary conditions are applied over
 271 the whole cross-sectional perimeter.

272 6.2. *Thermally developing flow*

273 The mathematical model is also validated with experimental evidences
 274 in case of thermally developing flow and fixed wall temperature boundary
 275 condition along the whole section perimeter. Except for the limiting case of
 276 circular duct, literature data are only provided in case of rectangular cross
 277 section channels and negligible viscous heating. Thus, Eqs. (21) and (13)
 278 are numerically solved. The case of rectangular cross section characterized
 279 by aspect ratio $\beta = 1/2$ is chosen. Since viscous heating is neglected, $Br = 0$,
 280 an uniform inlet temperature profile is imposed. The first 64 eigenfunctions,
 281 deriving from solution of eigenvalue problem, Eq. (26), are used for the
 282 imposition of inlet condition.

283 In figure 3, the resulting logarithmic Nusselt number Nu_l is plotted as a
 284 function of axial length and compared with experimental points printout in
 285 [34]. $Nu_l = h_l D_h/k$ can be easily computed by writing macroscopic energy
 286 balance,

$$\dot{Q}_w = \dot{m} c_p (T_i - T_b) = P x h_l \Delta T_l \quad (44)$$

287 ΔT_l being the logarithmic mean temperature:

$$\Delta T_l = \frac{\Delta T_i - \Delta T_b}{\log \left(\frac{\Delta T_i}{\Delta T_b} \right)} \quad (45)$$

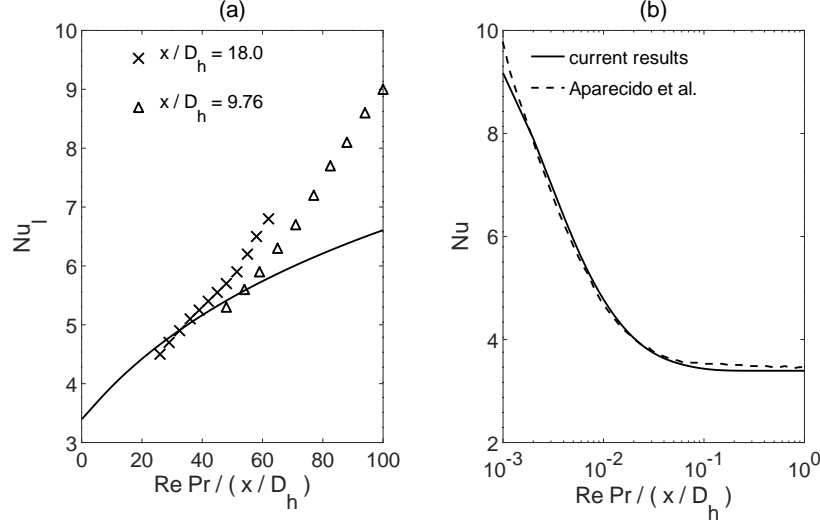


Figure 3: Computed logarithmic mean Nusselt number (continuous line) versus experimental data (markers) of [34] (a). Computed local Nusselt number versus numerical results of [26] along channel non-dimensional axial direction (b). T boundary condition, $\beta = 1/2$, $\gamma = 0$, $Br = 0$.

Expressing h_l through the energy balance and using non-dimensional quantities, the logarithmic mean Nusselt number becomes:

$$Nu_l = -\frac{1}{4} Re Pr \frac{D_h}{x} \log \Theta_b \quad (46)$$

It can be noticed that the logarithmic Nusselt number, as well as the bulk temperature along channel θ_b , univocally depends on the non-dimensional axial coordinate \tilde{x} :

$$\tilde{x} = \frac{x}{D_h} Re Pr \quad (47)$$

However, different values of Nu_l were experimentally obtained in [34] for a prescribed value of \tilde{x} , since experimental points are referred to different liquid flow rates \dot{m} . Such a discrepancy, which is not predicted by the mathematical

296 model, is due to the increasing Reynolds number, which is proportional to
 297 \dot{m} according to $\text{Re} = \dot{m} D_h / (\mu A_c)$, with higher values of the investigated Re
 298 approaching the laminar-turbulent transition value. In fact, the discrepancy
 299 between numerical and experimental results is lower than 10% for $\text{Re} < 10^3$.
 300 Figure 4 compares the resulting local Nusselt number, computed through Eq.
 301 (33), with the numerical results of [26], which authors numerically solved
 302 Eqs. (21) and (13), under the same boundary condition as here, using the
 303 generalized integral transform technique in order to reduce the costs of com-
 304 putations. A good agreement can be observed in both the entry region and
 305 the fully developed value of the Nusselt number.

306 **7. Results and discussion**

307 Equations (19) and (21) are numerically solved together with momentum
 308 equation, Eq. (13), and the resulting solutions Θ_c and Θ_v combined in order
 309 to define the temperature field Θ .

310 Numerical results shown in figures 4, 5 and 6 all refer to the conditions listed
 311 below, which have not been investigated so far in the open literature:

- 312 • Case 3T: rectangular section with 2 rounded corners and 3 edges heated,
 313 see Fig. 1(a);
- 314 • Inlet condition: adiabatic preparation, see Eqs. (22) and (23);
- 315 • Channel aspect ratio: $\beta = 3/5$;
- 316 • Non-dimensional joint radius: $\gamma = 2/3$;
- 317 • Graetz number: $\text{Gz} = 3.5$;

318 • Brinkman number: $Br = 0.1$.

319 Inlet temperature profile (i.e. at $x = 0$) is shown in Fig. 4(a), while fully de-
 320 veloped velocity and temperature profiles (corresponding to infinite channel
 321 length, $x \rightarrow \infty$) are shown in Figs. 4(b) and 4(c) respectively. Note that the
 322 imposed inlet temperature field, which derives from imposition of adiabatic
 323 preparation, is not uniform and requires additional numerical investigation.
 324 In fact $\Theta_0(\eta, \zeta)$ is not known a priori and Eq. (19) must be solved under
 325 adiabatic condition applied at channel section perimeter. Fig. 4(a) actually
 326 provides the numerically computed profile Θ_0 , which must be fitted using
 327 the eigenfunctions ψ_n from the solution of Eqs. (26) and (27) together with
 328 the contribution of Θ_v , in order to impose the inlet condition when solving
 329 energy equation inside the channel,

$$C_n : \min \left\{ \sum_i \epsilon_i^2 \right\}, \epsilon_i = \Theta_{0,i} - \sum_n C_n \psi_{n,i} \quad (48)$$

330 with i denoting the mesh element.

331 Actually, the first 50 eigenfunctions ψ_n deriving from Eq. (26) were used.
 332 Following the procedure of [23], where the number of eigenfunctions were set
 333 to 20 only, it was first verified that using 60 eigenfunctions instead of 50 does
 334 not lead to significant improvement (namely $< 0.01\%$) in terms of computed
 335 Nusselt number at $x/D_h > 0.001 Pe$, meaning that sufficient accuracy is
 336 reached. We decided to evaluate the accuracy on the estimated Nu , since
 337 it is the relevant quantity we want to extrapolate from computation so far.
 338 However, the truncation error,

$$\epsilon = \frac{|\Theta_0 - (\Theta_v + \sum_n C_n \psi_n)|}{|\Theta_0|} \quad (49)$$

339 was also computed for different numbers of ψ_n (needed to fit the imposed
 340 Θ_0), in order to verify the proper imposition of the desired inlet temperature
 341 profile, finding that $\epsilon_{50} = 0.1341$ (with the cross-section geometry discretized
 342 using more than 15000 triangular elements) and $\frac{\Delta\epsilon}{\Delta n} = \frac{\epsilon_{50}-\epsilon_{60}}{10} \simeq 1.1 \times 10^{-3}$
 343 (thus, the truncation error would slowly decrease for increasing number of
 344 eigenfunctions).

345 Looking at the fully developed temperature profile, figure 4(c), it is impor-
 346 tant to point out that the fluid becomes warmer than the duct at $x \rightarrow \infty$,
 347 owing to the effect of viscous heating. In fact, the fluid is progressively
 348 heated due to the heat exchange through duct walls in the thermal entrance
 349 region, whilst heat generation due to viscous dissipation (acting as source
 350 term in the energy equation) is the dominant effect when the bulk temper-
 351 ature approaches the imposed wall temperature T_w . Computed Poiseuille
 352 number, which is uniform along channel axial direction, assumes the value
 353 of $Po = 15.691$. Local Nusselt number along heated perimeter of the duct
 354 cross section is numerically computed from the fully-developed temperature
 355 profile. Comparing its behaviour, Fig. 5(b), to the corresponding channel
 356 section geometry, Fig. 5(a), it can be noticed that the maximum value of Nu
 357 is symmetrically reached along the two longer edges, where the temperature
 358 gradient is at its highest.

359 Non-dimensional temperature as a function of axial coordinate is also com-
 360 puted along the thermal entrance region. Figure 6(a) shows the temperature
 361 profile over the vertical mid-plane of the channel: as mentioned above, heat
 362 is transferred from the duct wall to the fluid flow until viscous heating be-
 363 comes the dominant effect driving heat transfer. The mean Nusselt number

364 along the channel length is numerically computed through Eqs. (30), (31)
 365 and (33) and is plotted in Fig. 6(b). The switch between convective heat
 366 exchange and dominating viscous heating can be identified by $Nu = 0$, which
 367 corresponds to $x/L \simeq 0.37$, whilst bulk temperature becomes higher than
 368 the imposed wall temperature after the vertical asymptote, $x/L \simeq 0.59$.
 369 As widely reported in literature [11, 24–27, 30], the profile of the mean Nusselt
 370 number is affected by several parameters:

- 371 • Brinkman number and Peclet number, $Pe = RePr$, defines the flow
 372 characteristics;
- 373 • aspect ratio and non-dimensional joint radius, which define the geom-
 374 etry of the cross-section .

375 Knowing the effect of such parameters is crucial in practical engineering
 376 problems involving micro-channels heat exchanger optimization [17–20].
 377 Lee et al. [27] proposed a correlation for predicting the mean Nusselt number
 378 as a function of axial coordinate in case of negligible viscous heating (i.e.
 379 $Br = 0$),

$$Nu_c \simeq \frac{1}{C_1 \tilde{x}^{C_2} + C_3} + C_4 \quad (50)$$

380 with \tilde{x} the non-dimensional axial coordinate:

$$\tilde{x} = \frac{x}{D_h} Pe^{-1} \quad (51)$$

Regression coefficients C_{1-4} are plotted in [27] as a function of the aspect ratio β defining the rectangular cross section.

Equation (50) is not sufficient for fitting the behaviour of the Nusselt number when the viscous heating source term plays a dominant role in heat transfer

process, see Fig. 6(b). Thus, a modified regression model is considered instead,

$$\text{Nu} \simeq \frac{\text{Nu}_v - \text{Nu}_c \chi}{1 - \chi} \quad (52)$$

$$\chi = \frac{C + \text{Br}}{\text{Br}} \exp \left[-m \frac{x}{D_h} \text{Pe}^{-1} \right] \quad (53)$$

where Nu_c can be calculated through Eq. (50).
Applying such a correlation, i.e. Eqs. (52) and (53), for fitting the numerical curve of Fig. 6(b) allows to reach a residual sum of square tolerance of 10^{-2} on 1000 computed values of Nu. Regression coefficient C and exponent m must be determined as a function of the channel cross-section geometry and of the Nusselt number at dominant viscous heating Nu_v . It was verified that the computed values of C and m are not affected by changing Peclet and Brinkman numbers while keeping the cross section geometry fixed, with a discrepancy of $\Delta C/C \sim 1\%$, $\Delta m/m \sim 1\%$ for $\text{Pe} \in [10^1, 10^3]$, $\text{Br} \in [10^{-3}, 10^{-1}]$. It is worth to point out that coefficients C_{1-4} , C and m are affected by the imposed inlet condition. In accordance to the work of Barletta et al. [23], an adiabatic preparation of the fluid $\Theta_0(\eta, \zeta)$ having bulk temperature $T_i < T_w$ is always considered throughout this paper.
The effect of changing the joint radius on the mean Nusselt number was investigated and the resulting curves are plotted in Figs.7(a) and 7(b), which are referred to fixed Brinkman number and cross section aspect ratio, for both test cases 3T and 4T. It can be noticed that the position x , at which transition between convective to viscous driven heat transfer occurs, decreases with increasing γ , in accordance with the effect of rounding the cross section geometry, which improves heat exchange process. As expected, the effect

γ	C	m	C_1	C_2	C_3	C_4	
0	0.7539	11.83	263.8	1.307	0.1668	3.597	3T
0.25	0.7582	12.26	270.9	1.310	0.1614	3.747	
0.5	0.7674	12.56	276.8	1.311	0.1588	3.859	
1	0.7632	12.60	281.5	1.312	0.1579	3.914	
0	0.9225	12.86	258.0	1.321	0.1674	3.168	4T
0.25	0.9344	13.82	276.1	1.329	0.1575	3.410	
0.5	0.9592	14.57	292.6	1.334	0.1527	3.597	
1	0.9878	15.07	335.9	1.352	0.1506	3.727	

Table 3: Regression coefficients of Eq. (53) for Nusslet number calculation through Eq. (52); $\beta = 3/5$.

of rounding on the computed Nu is stronger for test case 4T, corresponding to 4 rounded corners. The corresponding values of coefficients C_{1-4} , C and m , which allow fitting the numerical results of Figs.7(a) and 7(b) through Eqs. (50), (52) and (53), are reported in Table 3, while the dependence of thermal entrance length, L_{th} : $\text{Nu}(L_{th}) = 0.95 \text{Nu}_\infty$, on the Brinkman number and radius is shown in Fig. 8, where the non-dimensional thermal entrance length,

$$\tilde{L}_{th} = \frac{L_{th}}{D_h} \text{Pe}^{-1} \quad (54)$$

monotonically decreases for increasing Brinkman numbers in both test cases, 3T and 4T. Note that solution of Eqs. (19) and (26) for a given section geometry allows one to investigate Graetz-Brinkman problem for any value of Pe and Br and for any inlet temperature condition, eigenfunctions Θ_n only depending on duct section geometry and Θ_v being proportional to Brinkman

413 number magnitude.

414 Thermally developed temperature profiles, corresponding to computed so-
415 lution at $x > L_{th}$, through the duct cross section are shown in Fig. 9 for
416 $Br = 0.1$ and $\gamma = 0, 1$. Comparing Figs. 9(a), 9(b) to Figs. 9(c), 9(d) re-
417 veals that test case strongly influences the heat transfer process, since higher
418 temperatures are reached when only a portion of the cross section perimeter
419 is heated (test case 3T). On the other hand, the effect of rounding appears to
420 be much more important when the whole perimeter is heated (test case 4T).
421 The dependence of the fully-developed Nusselt number on channel geometry
422 and on both test cases is discussed further later on.

423 As a further validation, comparing Fig. 9(d) to the numerical results of
424 [33], where the Authors investigated the restrictive case of laminar, fully
425 developed flow with $Br \neq 0$ through a stadium-shaped channel (i.e. $\gamma = 1$)
426 with imposed wall temperature (corresponding to the current 4T test case),
427 reveals the same qualitative temperature profile.

Several simulations were run in order to trace both Poiseuille and Nusselt numbers of the fully (hydrodynamically and thermally) developed flow for different channel geometries, looking for accurate correlations. After a regression analysis, fourth order polynomial correlations were used to fit the fully developed Poiseuille and Nusselt numbers as a function of the non-dimensional joint radius:

$$Po = \sum_{m=1}^5 B_m \gamma^{m-1} \quad (55)$$

$$Nu_v = \sum_{m=1}^5 C_m \gamma^{m-1} \quad (56)$$

428 Coefficients B_{1-5} , C_{1-5} are reported for different channel aspect ratios β in

429 tables 4 and 5. Results for both test cases 3T and 4T are shown. Developed
 430 Poiseuille and Nusselt numbers are also plotted as a function of channel cross
 431 section geometry in Fig. 10, which clearly shows that the effect of rounding
 432 corners is relevant if 4 corners are rounded instead of 2 (i.e. when test case 4T
 433 is considered) and the imposed aspect ratio is sufficiently high. The heated
 434 perimeter length $\partial\Omega_h$ also plays an important role: comparing Fig. 10(c) to
 435 10(d) reveals that test case 3T may lead to higher Nusselt numbers than T4
 436 at small aspect ratio, while lower Nusselt numbers are obtained applying 3T
 437 constraint when $\beta > 1/2$.

438 8. Conclusion

439 In this paper the Poiseuille number and Nusselt, both local and average,
 440 number of a laminar, thermally developing flow of a Newtonian fluid inside
 441 a rectangular microchannel with rounded corners were studied. The effect
 442 of viscous heating was taken into account, leading to the so-called Graetz-
 443 Brinkman problem, and T boundary conditions were applied along the heated
 444 perimeter of the channel cross section.

445 Numerical simulations were conducted using MATLAB[®] pdetool, a finite-element
 446 based solver, in order to compute velocity and temperature fields over the
 447 3D channel domain. After a proper validation with literature data, several
 448 configurations involving complex channel section geometries, most of them
 449 never considered in the available literature, were investigated through an ef-
 450 ficient numerical method in terms of computational costs, looking for new
 451 correlations for Poiseuille and Nusselt number prediction. In particular, novel
 452 correlations taking into account viscous heating were proposed for: calcula-

tion of Nusselt number along channel axial direction in the thermal entrance region, Eqs. (52) and (53); calculation of the developed Poiseuille and Nusselt numbers, Eqs. (55) and (56). Also, the effects of the Brinkman number, heated cross section perimeter and channel geometry (defined by aspect ratio and rounding radius) on heat transfer performances were studied and a connection between thermal entrance length and Brinkman number was found. The results obtained may be useful for microchannel heat sinks design according to Performance Evaluation Criteria [15], since the Poiseuille and average Nusselt numbers are required for evaluation of transferred heat power, friction loss and Entropy Generation Number [16].

As future work, rarefied fluid flows will be studied since rarefaction effects as well as viscous dissipation may be non-negligible at the microscale [8]; a general Robin boundary condition depending on Knudsen number Kn (which is the ratio between molecular mean free path and hydraulic diameter) must be imposed over the perimeter or its heated part, depending on whether the velocity or the temperature fields are investigated. Also the laminar flow of non-Newtonian fluids characterized by power-law viscosity and significant viscous dissipation should be analysed, since they represents a physical problem involved in many engineering applications.

References

- [1] M. Ohadi, K. Choo, S. Dessiatoun, and E. Cetegen. *Next Generation Microchannel Heat Exchangers*. Springer, Heidelberg, 2013.
- [2] M. Spiga and G.L. Morini. Nusselt numbers in laminar flow for h2 boundary conditions. *Int. J. Heat Mass Tran.*, 39:1165, 1996.

- 477 [3] G.L. Morini. Viscous heating in liquid flows in micro-channels. *Int. J.*
478 *Heat Mass Tran.*, 48:3637, 2005.
- 479 [4] M. Geri, M. Lorenzini, and G.L. Morini. Effects of the channel geometry
480 and of the fluid composition on the performances of dc electro-osmotic
481 pumps. *International Journal of Thermal Sciences*, 55:114, 2007.
- 482 [5] M. Lorenzini. The influence of viscous dissipation on thermal perfor-
483 mance of microchannels with rounded corners. *Le Houille Blanche*, 4:64,
484 2013.
- 485 [6] M. Lorenzini and G. L. Morini. Single-phase laminar forced convection
486 in microchannels with rounded corners. *Heat Transfer Eng.*, 32:1108,
487 2011.
- 488 [7] P. Vocale, G.L. Morini, and M. Spiga. Dilute gas flows through elliptic
489 microchannels under h2 boundary conditions. *Int. J. Heat Mass Tran.*,
490 71:376, 2014.
- 491 [8] P. Vocale, G.L. Morini, M. Spiga, and S. Colin. Shear work contribution
492 to convective heat transfer of dilute gases in slip flow regime. *Eur. J.*
493 *Mech. B-Fluid*, 64:60, 2017.
- 494 [9] C. Aubert and S. Colin. High-order boundary conditions for gaseous
495 flows in rectangular microducts. *Microscale Therm. Eng.*, 5:41, 2001.
- 496 [10] S. Colin, P. Lalonde, and R. Caen. Validation of a second-order slip flow
497 model in rectangular microchannels. *Heat Transfer Eng.*, 25:23, 2004.

- 498 [11] B. Çetin, A.G. Yazıcıoğlu, and S. Kakaç. Slip-flow heat transfer in
499 microtubes with axial conduction and viscous dissipation – an extended
500 graetz problem. *Int. J. Therm. Sci.*, 48:1673, 2009.
- 501 [12] J. Koo and C. Kleinstreuer. Liquid flow in microchannels: Experimental
502 observations and computational analyses of microfluidics effects. *Journal*
503 *of Micromechanics and Microengineering*, 13(5):568–579, 2003.
- 504 [13] A. Sadeghi, M.H. Saidi, and A.A. Mozafari. Heat transfer due to elec-
505 troosmotic flow of viscoelastic fluids in a slit microchannel. *Int. J. Heat*
506 *Mass Tran.*, 54(17-18):4069–4077, 2011.
- 507 [14] M. Lorenzini, I. Daprà, and G. Scarpi. Heat transfer for a giesekus
508 fluid in a rotating concentric annulus. *Applied Thermal Engineering*,
509 122:118–125, 2017.
- 510 [15] R. L. Webb. *Principles of Enhanced Heat Transfer*. Wiley, New York,
511 1994.
- 512 [16] A. Bejan. *Entropy generation through heat and fluid flow*. Wiley, New
513 York, 1982.
- 514 [17] V. Zimparov. Extended performance evaluation criteria for enhanced
515 heat transfer surfaces: heat transfer through ducts with constant wall
516 temperature. *Int. J. Heat Mass Tran.*, 43:3137, 2000.
- 517 [18] V. Zimparov. Extended performance evaluation criteria for enhanced
518 heat transfer surfaces: heat transfer through ducts with constant heat
519 flux. *Int. J. Heat Mass Tran.*, 44:169, 2001.

- 520 [19] S. Chakraborty and S. Ray. Performance optimization of laminar fully
521 developed flow through square ducts with rounded corners. *Int. J.*
522 *Therm. Sci.*, 50:2522, 2011.
- 523 [20] M. Lorenzini and N. Suzzi. The influence of geometry on the thermal
524 performance of microchannels in laminar flow with viscous dissipation.
525 *Heat Transfer Eng.*, 37:1096, 2016.
- 526 [21] S. Ray and D. Misra. Laminar fully developed flow through square and
527 equilateral triangular ducts with rounded corners subjected to h1 and
528 h2 boundary conditions. *Int. J. Therm. Sci.*, 49:1763, 2010.
- 529 [22] G.L. Morini, M. Spiga, and P. Tartarini. The rarefaction effect on
530 the friction factor of gas flow in microchannels. *Superlattice. Microst.*,
531 35:587, 2004.
- 532 [23] A. Barletta and E. Magyari. The graetz-brinkman problem in a plane-
533 parallel channel with adiabatic-to-isothermal entrance. *Int. Comm. Heat*
534 *Mass*, 33:677, 2006.
- 535 [24] M.L. Michelsen and J. Villadsen. The graetz problem with axial heat
536 conduction. *Int. J. Heat Mass Tran.*, 17:1391, 1974.
- 537 [25] T. Basu and D.N. Roy. Laminar heat transfer in a tube with viscous
538 dissipation. *Int. J. Heat Mass Tran.*, 28:699, 1985.
- 539 [26] J.B. Aparecido and R.M. Cotta. Thermally developing laminar flow
540 inside rectangular ducts. *Int. J. Heat. Mass Tran.*, 33:341, 1990.

- 541 [27] P.S. Lee and S.V. Garimella. Thermally developing flow and heat trans-
542 fer in rectangular microchannels of different aspect ratios. *Int. J. Heat*
543 *Mass Tran.*, 49:3060, 2006.
- 544 [28] A. Filali, L. Khezzar, D. Siginer, and Z. Nemouchi. Graetz problem with
545 non-linear viscoelastic fluids in non-circular tubes. *Int. J. Therm. Sci.*,
546 61:50, 2012.
- 547 [29] O. Aydin and M. Avci. Laminar forced convective slip flow in a microduct
548 with a sinusoidally varying heat flux in axial direction. *Int. J. Heat Mass*
549 *Tran.*, 89:606, 2015.
- 550 [30] M. Barışık, A.G. Yazıcıoğlu, B. Çetin, and S. Kakaç. Analytical so-
551 lution of thermally developing microtube heat transfer including axial
552 conduction, viscous dissipation, and rarefaction effects. *Int. Commun.*
553 *Heat Mass*, 67:81, 2015.
- 554 [31] R. K. Shah and A. L. London. *Laminar Flow Forced Convection in*
555 *Ducts - A Source Book for Heat Exchanger Analytical Data*. Academic
556 Press, New York, 1978.
- 557 [32] J. B. Miles and J. Shih. Reconsideration of nusselt number for laminar
558 fully developed flow in rectangular ducts. an unpublished paper, 1967.
- 559 [33] A. Barletta and E. R. di Schio. Analysis of the effect of viscous dissi-
560 pation for laminar flow in stadium-shaped ducts. *Int. Commun. Heat*
561 *Mass*, 28:449, 2001.
- 562 [34] P. Wibulswas. *Laminar flow heat transfer in non-circular ducts*. PhD
563 thesis, University College London, 1966.

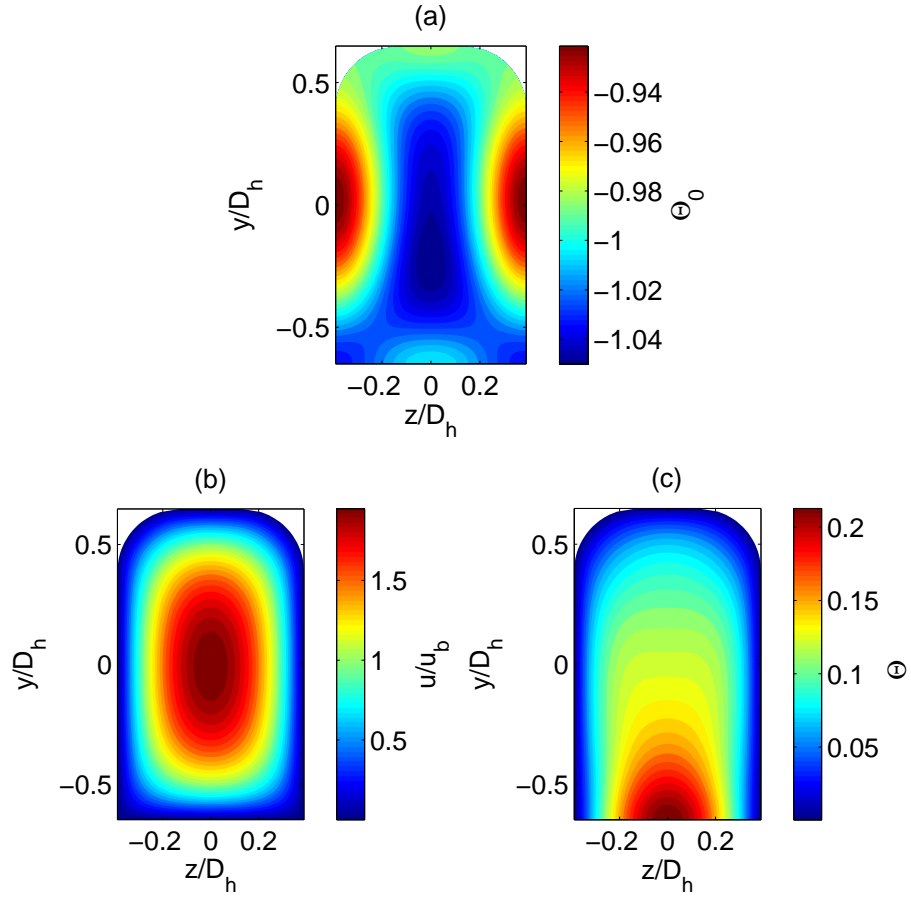


Figure 4: Inlet temperature profile (a), developed velocity profile (b) and developed temperature profile (c). $Br = 0.1$, $\beta = 3/5$, $\gamma = 2/3$.

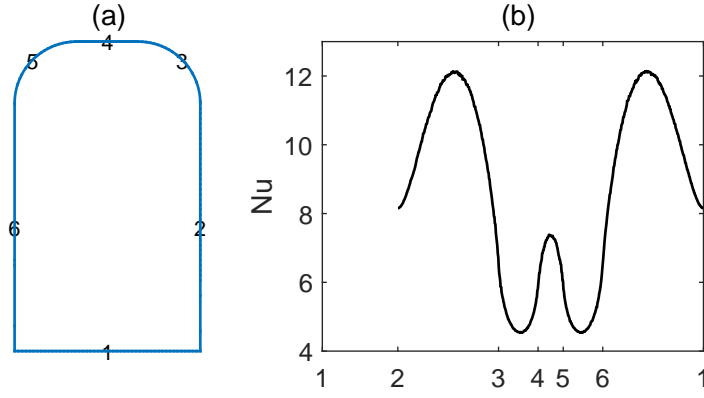


Figure 5: Channel section geometry (a) and local Nusselt number along heated perimeter (b). $\beta = 3/5$, $\gamma = 2/3$.

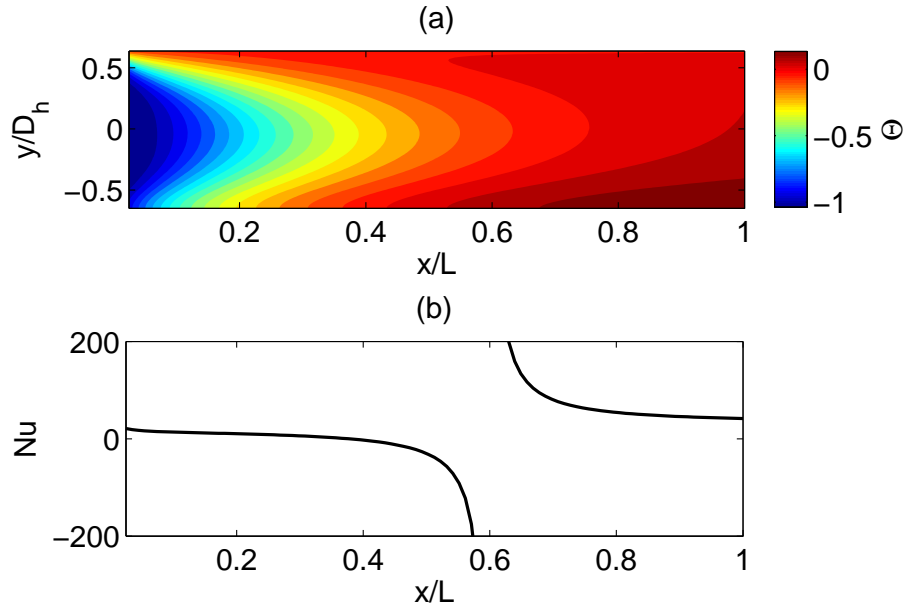


Figure 6: Temperature profile across symmetry section $z = 0$ (a) and mean Nusselt number as a function of axial coordinate (b). $Gz = 3.5$, $Br = 0.1$, $\beta = 3/5$, $\gamma = 2/3$.

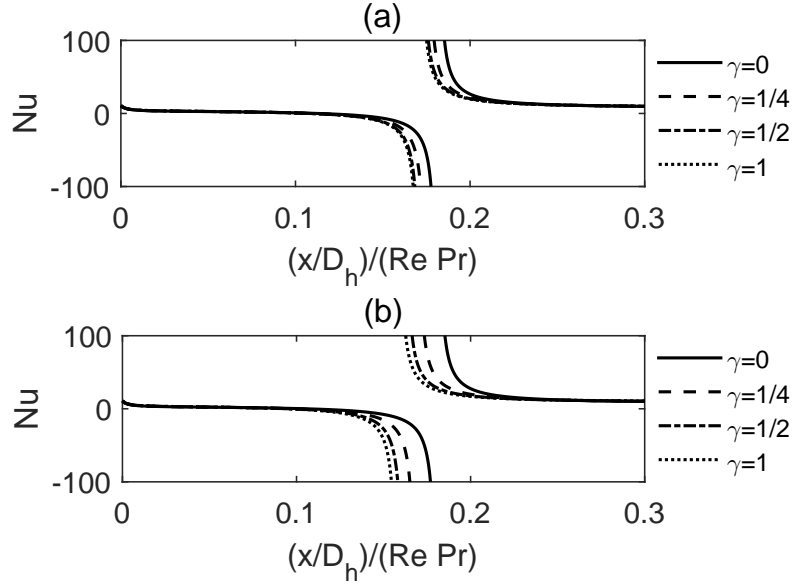


Figure 7: Nusselt number as a function of axial coordinate and non-dimensional joint radius for test cases 3T (a) and 4T (b). $\beta = 3/5$, $Br = 0.1$.

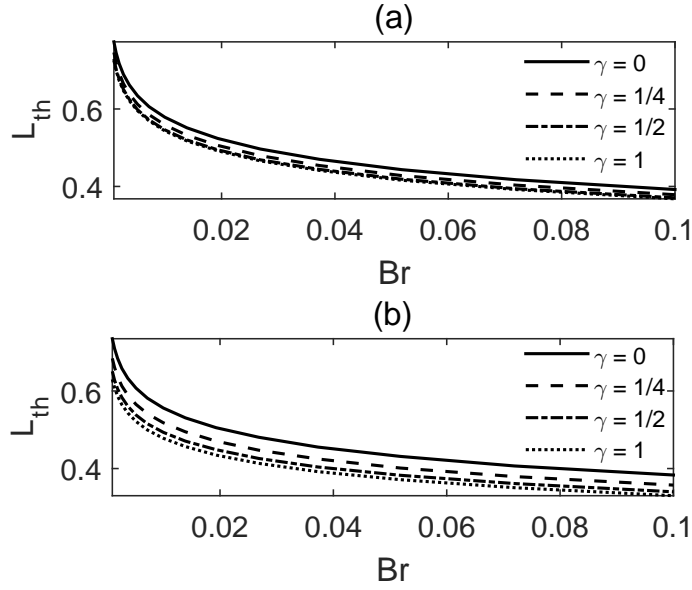


Figure 8: Non-dimensional length of the thermal entrance region as a function of Brinkman number and corner rounding radius: test case 3T (a); test case 4T (b). $\beta = 3/5$.

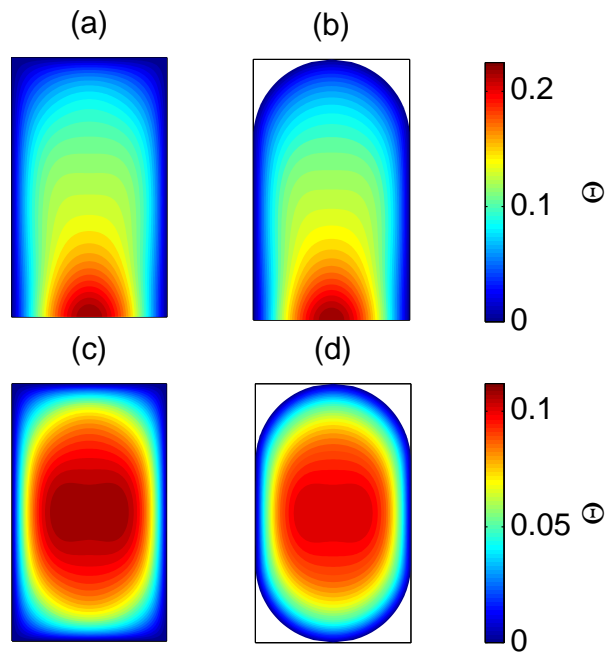


Figure 9: Developed temperature profile for different test cases and cross section geometries: $\gamma = 0$, 3T (a); $\gamma = 1$, 3T (b); $\gamma = 0$, 4T (c); $\gamma = 1$, 4T (d). $\beta = 3/5$, $Br = 0.1$

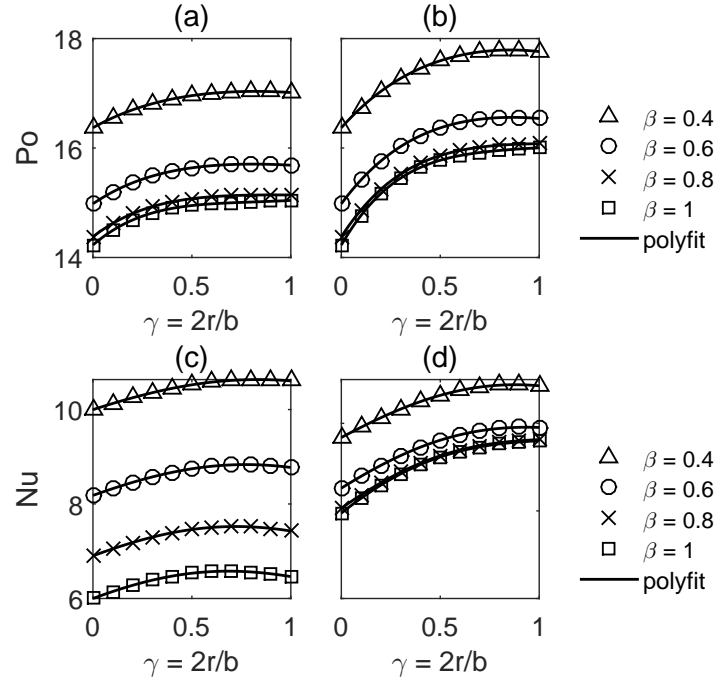


Figure 10: Numerical data vs Eqs. (55) and (56) describing developed Poiseuille and Nusselt numbers as a function of non-dimensional rounding radius and aspect ratio: Po for test case 3T (a); Po for test case 4T (b); Nu_v for test case 3T (c); Nu_v for test case 4T (d).

β	B_1	B_2	B_3	B_4	B_5	
0.05	22.48	0.4619	-0.3860	0.1602	-0.04336	3T
0.1	21.17	0.8320	-0.7220	0.3068	-0.08366	
0.2	19.07	1.376	-1.281	0.5655	-0.1532	
0.3	17.51	1.753	-1.755	0.8191	-0.2203	
0.4	16.37	2.032	-2.186	1.085	-0.2875	
0.5	15.55	2.256	-2.603	1.382	-0.3590	
0.6	14.98	2.451	-3.026	1.718	-0.4393	
0.7	14.61	2.628	-3.455	2.086	-0.5261	
0.8	14.38	2.796	-3.898	2.489	-0.6240	
0.9	14.26	2.959	-4.360	2.930	-0.7383	
1.0	14.23	3.118	-4.837	3.404	-0.8709	
0.05	22.48	0.9239	-0.7573	0.3062	-0.08221	4T
0.1	21.17	1.664	-1.398	0.5753	-0.1580	
0.2	19.07	2.753	-2.432	1.022	-0.2825	
0.3	17.51	3.509	-3.285	1.439	-0.3939	
0.4	16.37	4.068	-4.047	1.866	-0.4950	
0.5	15.55	4.518	-4.781	2.332	-0.5889	
0.6	14.98	4.908	-5.532	2.877	-0.6942	
0.7	14.61	5.264	-6.302	3.481	-0.8095	
0.8	14.38	5.604	-7.122	4.187	-0.9684	
0.9	14.26	5.938	-8.014	5.043	-1.214	
1.0	14.23	6.278	-9.030	6.157	-1.629	

Table 4: Regression coefficients of Eq. (55) for polynomial fit of Po as a function of γ .

β	C_1	C_2	C_3	C_4	C_5	
0.05	16.09	0.3325	-0.07389	-0.1167	0.03890	3T
0.1	14.86	0.5955	-0.1398	-0.2059	0.06557	
0.2	12.82	0.9630	-0.2258	-0.3657	0.1131	
0.3	11.23	1.192	-0.2780	-0.5037	0.1604	
0.4	9.999	1.339	-0.3287	-0.5974	0.1948	
0.5	9.005	1.433	-0.3774	-0.6692	0.2245	
0.6	8.181	1.490	-0.4233	-0.7305	0.2552	
0.7	7.487	1.522	-0.4667	-0.7846	0.2900	
0.8	6.902	1.538	-0.5174	-0.8190	0.3240	
0.9	6.410	1.546	-0.5727	-0.8400	0.3598	
1.0	5.998	1.551	-0.6411	-0.8375	0.3914	
0.05	15.85	0.6514	-0.1568	-0.2019	0.06138	4T
0.1	14.46	1.133	-0.2430	-0.4073	0.1229	
0.2	12.28	1.763	-0.3372	-0.7391	0.2197	
0.3	10.73	2.141	-0.4107	-0.9544	0.2908	
0.4	9.677	2.400	-0.4949	-1.089	0.3644	
0.5	8.977	2.610	-0.6096	-1.160	0.4451	
0.6	8.520	2.803	-0.7648	-1.182	0.5302	
0.7	8.232	2.994	-0.9619	-1.162	0.6126	
0.8	8.061	3.190	-1.211	-1.080	0.6696	
0.9	7.975	3.395	-1.535	-0.8914	0.6611	
1.0	7.949	3.613	-1.955	-0.5454	0.5408	

Table 5: Regression coefficients of Eq. (56) for polynomial fit of Nu_v as a function of γ .